ORIGINAL RESEARCH

CONTROLLABLE CORE SIZE OF Au@TiO$_2$ THROUGH Al(NO$_3$)$_3$ ADDITION AND ITS EFFECTS ON DSSC PERFORMANCE

Sangsaka Wira Utama[1] | Rachmat Hidayat[1] | Nur Fadhilah[1] | Muhammad Husain Haekal*[1] | Rozalina Zakaria[2] | Rachmat Hidayat[3] | Doty Dewi Risanti[1]

[1]Dept. of Physics Engineering, Institut Teknologi Sepuluh Nopember, Surabaya, Indonesia

[2]Dept. of Physics, University of Malaya, Kuala Lumpur, Malaysia

[3]Dept. of Physics, Institut Teknologi Sepuluh Nopember, Surabaya, Indonesia

Correspondence

*Muhammad Husain Haekal, Dept of Physics Engineering, Institut Teknologi Sepuluh Nopember, Surabaya, Indonesia. Email: haekal@its.ac.id

Present Address

Gedung Teknik Fisika, Jl. Raya ITS, Surabaya 60111, Indonesia

Abstract

It is known that plasmonic nanoparticles in dye-sensitized solar cells (DSSC) could enhance efficiency through improvement in light absorbance and electron dynamics. Herein we investigated various sizes of AuNP through spontaneous Al(NO$_3$)$_3$ addition. Core-Shell Au@TiO$_2$ was prepared with various Al(NO$_3$)$_3$ concentrations of 0.25 mM, 0.5 mM, 0.75 mM and 1 mM. The Au@TiO$_2$ volume fraction of 1% was further added to TiO$_2$ photoanode. Based on the particle size analyzer (PSA) characteristics, the synthesized AuNP's size was within a range of 34.62 nm – 139.5 nm. The highest efficiency of DSSC was obtained for the sample with the largest AuNP 's diameter, i.e., 0.0313%, which is about three times higher than pristine DSSC. The increase in efficiency was in accord with Metallic Nanoparticle Boundary Element Method (MNPBEM) simulation, UV-vis spectroscopy, and Incident Photon to Current Conversion Efficiency (IPCE) analysis largest Au core diameter contributes to the strong absorbance and hence the short circuit current.

KEYWORDS:

Core-Shell, DSSC Performance, Nanoparticle, Photoanode, Plasmonic

1 | INTRODUCTION

Several ways can be done to improve the efficiency of Dye-Sensitized Solar Cells (DSSC) by adding metal in a core-shell structure into the photoanode. It is known that by incorporating core-shell of metal encapsulated by oxide, the localized surface plasmons resonance (LSPR) becomes feasible and increases the absorption of the dye molecules. Hence improvement in electron collection and device performance can be obtained. There are metals commonly used for promoting LSPR in the visible region, i.e., gold (Au)[1, 2], silver (Ag)[3], copper (Cu)[4], and bismuth (Bi)[5], among which Au is the most excellent metal exhibiting

strong LSPR effect. The way LSPR works in DSSC is as follows, the metallic core concentrates light. At the same time, the shell ought to provide optimal spacing, chemical stability, good electrical conductivity, and good photovoltaic properties.

Therefore, the morphology of the core, the material used, and the thickness of the shell need to be carefully designed and controlled to obtain optimal enhancement[6, 7]. Typically, the enhancement effect of metal@dielectric core-shell nanoparticles is attributed to the enhanced excitation rate of dye sensitizers due to LSPR. Even though the metal nanoparticles can be protected and hindered from charge recombination, one may expect two beneficial mechanisms involved in the efficiency enhancement for using TiO_2 semiconductor as the shell. First, the hot electrons generated inside the resonant plasmonic cores can contribute directly to the photocurrent. Second, the metal cores can undergo charge equilibrium with the surrounding semiconductor and modify the Fermi level of TiO_2, resulting in an improved cell potential[1].

Extensive studies focusing on the prevention of recombination and improving charge transfer efficiency through incorporation of metals such as copper[8, 9], gold[10], silver[11, 12], palladium[13], or platinum[14] in DSSC photoanode have been reported. The noble metals offer advantages due to their resonance in the visible region and stability, where Cu is unstable against surface oxides, while Pd and Pt show very weak resonance[15]. Au and Ag have quite strong resonance among these metals due to the enhanced extinction cross-section and the tunability of plasmon resonance by the surrounding. In comparison to Ag, Au possesses many benefits, particularly it has high stability either chemically or biologically, high sensitivity by the high surface-to-volume ratio, easy probe, and many more[16].

Intending to modify the core-shell morphology, this research focused on changing the core size without changing the amount of Au loading at a constant shell thickness. For this purpose, $Al(NO_3)_3$ was employed since it has been known that it can be used as a template for AuNP growth, either being added at a constant concentration[17] or being varied in proportional to the amount of AuNP loading[18]. The latter has shown that the growth of AuNP can be controlled by manipulating the amount of reducing agent of $HAuCl_4$. As the function of the reducing agent is limited, the mechanism is then controlled by the van der Waals attractive force leading to the integration of small AuNPs into aggregated AuNPs[19]. With these structures, we systematically studied the influence of Au core size on the plasmonic enhancement effect in DSSCs. Additionally, we report the effect of metallic core size using a simulation of metallic nanoparticles embedded in a dielectric medium using the boundary element method (BEM) approach. Finally, solar cell performance is investigated and analyzed concerning the controlled nanoscale light-matter interaction.

2 | PREVIOUS RESEARCHES

Many studies integrate AuNP coated with a thin shell either of silica or TiO_2 into the TiO_2 mesoporous paste. The intense absorption of AuNP due to its surface plasmon resonance depends on its size and shape[20, 21]. The control of size was mostly adjusted by using a sophisticated method[2] or simply by varying the volume fraction of Au and TiO_2 loading[22]. The use of $Al(NO_3)_3$ to control the growth of Au was firstly reported by[18] and explained thoroughly by[17]. By employing sacrificial hydrothermal reaction, the following reactions occur[23, 24] :

$$HAuCl_4 + OH - +4H+ \rightarrow Au + H_2O + 4HCl \left(\Delta G = -1316.24 \frac{kJ}{mol} \right) \tag{1}$$

$$Al(NO_3)_3.9H_2O + Al_3 + +6OH - +3H+ \rightarrow Al_2O_3 + 3H_2O \left(\Delta G = -711.82 \frac{kJ}{mol} \right) \tag{2}$$
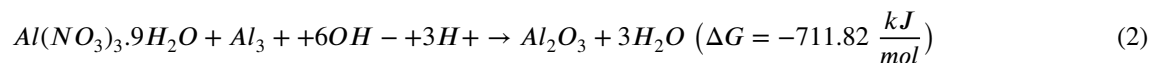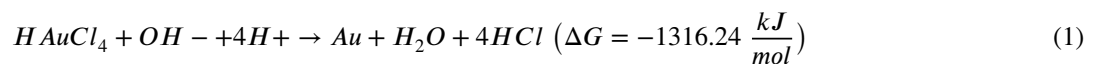
According to the free Gibbs energy formation (ΔG) of the above reactions, the formation of AuNP is easier due to its more negative energy. The AuNP will be formed heterogeneously on the grain boundary sites of Al. As reported in[17], the size of AuNP was adjusted by increasing the concentration of $HAuCl_4$. In this research, the number of heterogeneous nucleation sites was varied. Hence, the further growth and coarsening of the nuclei will be affected, too, through the Ostwald ripening phenomenon.

3 | MATERIAL AND METHOD

3.1 | Synthesis of Au@TiO₂ Core-Shell Photoanodes

TiO$_2$ photoanode powder was fabricated using the coprecipitation method and calcined at 600oC for 5 hours to get the anatase phase. AuNP with various diameters size was synthesized through the addition of different concentrations of Al(NO$_3$), i.e. 0.25 mM, 0,5 mM, 0,75 mM and 1 mM. Au@TiO$_2$ core-shell powder was obtained by mixing the AuNP with Ti4+ solution through a combination of TTIP (Titanium Isopropoxide) and TEOA (Triethanolamine) in a nitrogen atmosphere at a molarity ratio of 2:1 (TEOA: TTIP). The washing process of Au@TiO$_2$ took two weeks using equates. Subsequently, the powder of Au@TiO$_2$ photoanodes was calcined for 48 hours at 80o C.

3.2 | Characterization of Synthesized Au@TiO₂ Core-Shell Photoanodes

The particle size distribution of AuNP was carried out using a particle size analyzer (PSA) (Malvern Zetasizer). The crystal structure of photoanodes powder was characterized using X-ray diffraction (XRD) (Philips XPert MPD 30 mA, 40 kV) with Cu Kα radiation ($\lambda = 0.15406$ nm) with 2θ scanned within the range of 15°-90°. Absorption of photoanode powder in visible light (200 nm - 800 nm) was characterized using UV-Vis spectrophotometer Perkin-Elmer Lambda 750 UV / Vis / NIR. Raman spectra were obtained using a Renishaw inVia Raman Microscope (Wotton-under-Edge, UK) operating with NIR diode laser emitting at 785 nm. Spectra were recorded with an accumulation of one scan, 10 s exposure. To find out the morphology and core-shell structure, the sample was characterized using a field-emission scanning electron microscope (FE-SEM) JEOL JIB 4610F. Plasmonics simulation was undertaken using MATLAB equipped with MNPBEM (Metallic Nanoparticles Boundary Element Method) toolbox[25]. The toolbox works in principle for homogeneous dielectric bodies inside homogeneous dielectric surroundings, in which abrupt interfaces separate the bodies. In this paper, we simulated various Au diameters inside air surroundings. Photocurrent – voltage curves were measured under 100 mW/cm^2 using a solar simulator connected to PXI-E1073 and SMU PXI-4130 and LabView Software. The energy conversion efficiency (η) was calculated using Eq. 3.

$$\eta = \frac{J_{sc} \times V_{oc} \times FF}{P_i n} \tag{3}$$

Jsc is short circuit current density, Voc is open-circuit voltage, FF is filling factor, and Pin is the power input. Jmax is the current density at maximum power output, and Vmax is the voltage at maximum power output. The fill factor can be obtained by the Eq. 4.

$$FF = \frac{J_{max} \times V_{max}}{J_{sc} \times V_{oc}} \tag{4}$$

Incident photon to current conversion efficiency (IPCE) in the visible light spectrum was obtained by adjusting the wavelength of the incident light, i.e., a series connection of halogen lamp (GR-150 Halogen Flood Light 150W) and monochromator (CT-10T, JASCO). The value of incident light power was measured by using an optical power meter (Thorlab S-120C).

3.3 | Fabrication of DSSC

Photoanodes powder weighed 0.25 grams was made into pasta by dissolution in 87.5 μL in distilled water, 125 μL of CH3COOH, and 12.5 μL of Triton X-100. The coating of photoanode paste into FTO glass was undertaken by using the doctor blade method. Subsequently, the coated FTO glass was heated at 225oC for 2 minutes using a hot plate. The coated FTO glass was then soaked in a ruthenium complex N-719 dye solution for 12 hours. Finally, DSSC components with sandwich structures were made by arranging FTO glass coated with dyed-photoanode, an electrolyte solution, and a platinum-plated FTO glass as a counter electrode.

The sample used in this research is a concrete cylinder with a diameter of 100 x 200 mm. The materials used in this research are normal concrete which is made with ordinary portland cement, silica fume, and fly ash, with Console SS-8 as High Range Water Reducer (HRWR). The typical chemical composition of ordinary portland cement powder, silica fume, and fly ash is given in Tables 1 and Table 2 .
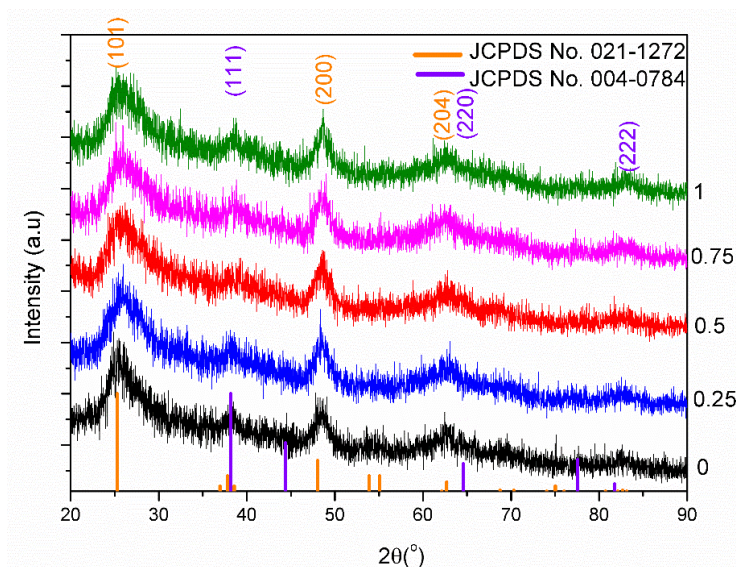
FIGURE 1 XRD spectra of Au@TiO$_2$ with various Al(NO$_3$)$_3$ used.
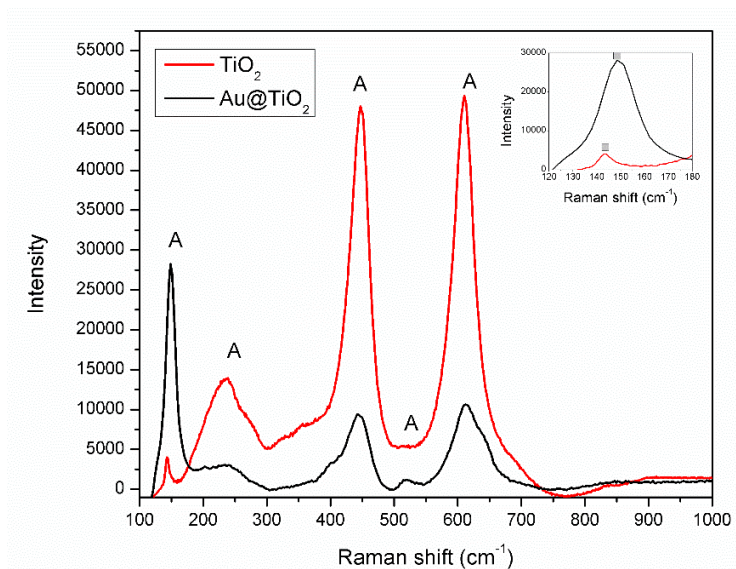
FIGURE 2 Raman spectra in the range of 100-1000 cm-1 for the Au@TiO$_2$ and Al(NO$_3$)$_3$.

4 | RESULTS AND DISCUSSION

Fig 1 shows XRD patterns of the Au@TiO$_2$ core-shell samples with Al(NO$_3$)$_3$ addition. As the XRD profile shows, the crystal planes of TiO$_2$ were mainly (101) planes, while the other peaks can be ascribed to the (200) and (204) planes (JCPDS No.021-1272). At the same time, the other diffraction peaks can be ascribed to the (111), (220), and (222) planes of Au (JCPDS No.004-0784). These results are related to the formation mechanism of the core-shell Au@TiO$_2$, i.e., the Au core predominantly grew in the (111) crystal planes. However, the peak intensity remains as the amount of Al(NO$_3$)$_3$ increases, while the TiO$_2$ grew profoundly in the (101) crystal planes, and it seems any changes in Au core do not alter the TiO$_2$ peaks.

Raman spectroscopy within the range of 100-1000 cm-1 was undertaken on pure TiO$_2$ and Au@TiO$_2$ with one mM Al(NO$_3$)$_3$ samples to evaluate the phases present in the prepared samples, and the results are shown in Fig 2 . Typical Raman peaks associated with anatase phase TiO$_2$ are detected[12]. Most of the peak intensities decreased and were shifted to a higher wavenumber

TABLE 1 The particle size of $Au - NP$ and Au@TiO$_2$.

Al(NO$_3$)$_3$ Concentration (mM)	Average Diameter of AuNP (nm)	Average Diameter of Core-Shell (nm)
0.00	34.62	304.7
0.25	43.31	346.7
0.50	48.49	237.6
0.75	81.23	303.8
1.00	139.8	285.8

(a) (a)   **(b)** (b)
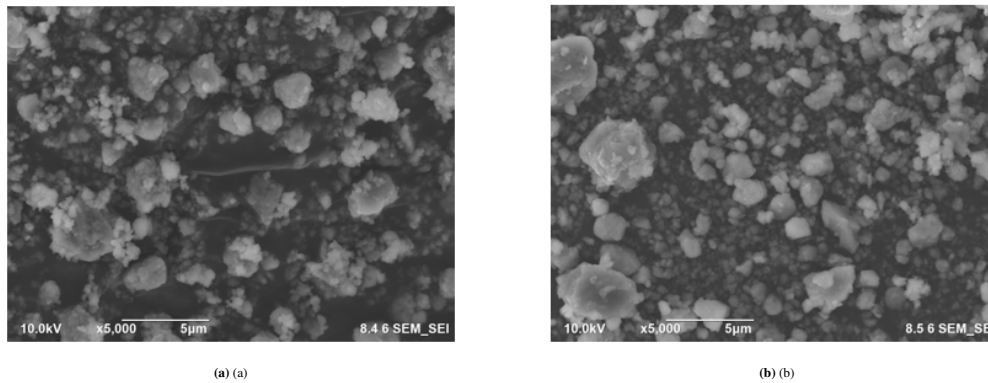
FIGURE 3 Secondary electron images of Au@TiO$_2$ with (a) 0.5 mM and (b) 1 mM Al(NO$_3$)$_3$ addition.
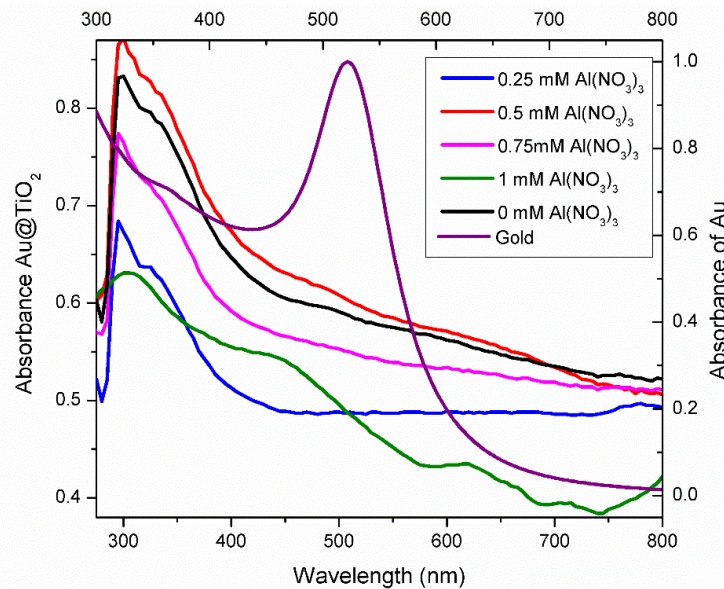
FIGURE 4 UV-Vis absorption spectra of core-shell Au@TiO$_2$ with the addition of Al(NO$_3$)$_3$.

as in Au@TiO$_2$. For instance, a band at about 144 cm-1 that corresponds to the external vibration of the $Ti - O$ bond shifts towards a higher wavenumber. This indicates an interaction between the Au and TiO$_2$, leading to an increase in the $Ti - O$ bond force constant due to reducing the $Ti - O$ bond length[26, 27]. Raman spectra of Au@TiO$_2$ may indicate that the Au nanoparticle is in the form of Au@TiO$_2$, and there is no such phase transformation, rather than an electronic environment change in the surroundings[28].

PSA characterization was undertaken for AuNPs only and Au@TiO$_2$ core-shell. The measurement of AuNP can be done directly because it was in the form of a liquid colloid. The samples had to be dissolved in 10 ml aquabidest per 5 mg powder for other
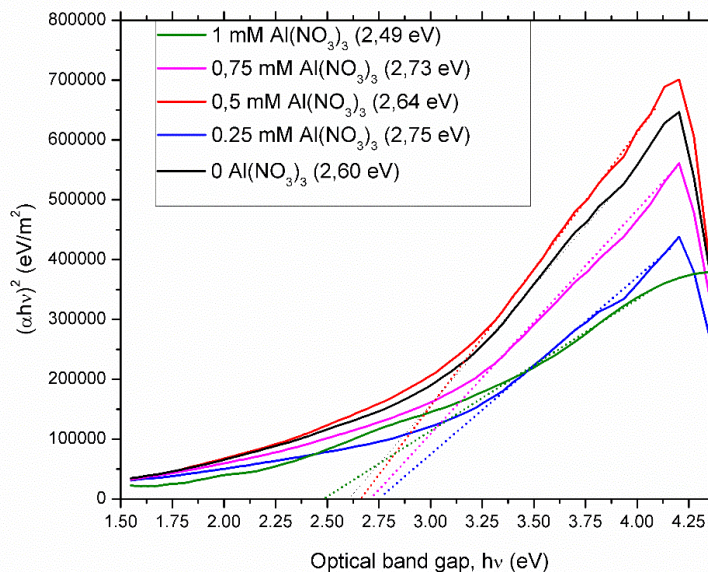
FIGURE 5 Tauc plot of Au@TiO$_2$ core-shell with the addition Al(NO$_3$)$_3$.

samples in the form of powder. The obtained average sizes of core and shell are tabulated in Table 1 . It is seen that the addition of Al(NO$_3$)$_3$ results in the further growth of AuNP . All samples studied typically show two distinct peaks of core-shell diameter due to the faster reduction process of *HAuCl*, leading to the formation of a heterogeneous population of AuNP[29]. Similar results were obtained from FE-SEM images (Fig 3).

According to UV-Vis characterization (Fig 4), all samples studied show weak surface plasmon resonance response (520 to 600 nm) as indicative of the thick TiO$_2$ shells for individual core-shell Au@TiO$_2$[30]. All samples reveal a strong peak belongs to TiO$_2$ at 320 nm, which remains unchanged with the addition of Al(NO$_3$)$_3$. Except for sample with one mM Al(NO$_3$)$_3$ shows three sluggish peaks 420 nm, 630 nm, and 700 nm, attributed to a strong interaction between Au and TiO$_2$, resonance absorption, and interband electronic transition, respectively[31]. Similar to Yao et al.[31], Au cores having a diameter less than 100 nm do not show any significant variation of optical absorption properties induced by Au cores. This may imply that small Au cores do not respond to the incident light.

UV-Vis characterization can also indicate the quality of the core-shell structure, whether the shell may or not cover the whole core. Since the absorption produced by the TiO$_2$ maintains the constant characteristics, this may suggest that the optical properties of the TiO$_2$ shell are not affected by the size of Au cores. The diminution of absorption intensity led by the electronic transition between Au cores and the TiO$_2$ shells for a sample having a core diameter less than 100 nm may indicate that the interaction between Au cores and TiO$_2$ shells is weakened as the shells fully cover the cores. The redshift of resonance absorption peak observed for samples with core diameter >100 nm may indicate that The TiO$_2$ shells coat Au cores. This redshift arises because TiO$_2$, as the dielectric environment of Au has a higher refractive index, i.e., 2.5. As the TiO$_2$ shells coat Au cores, the absorption induced by the interband transition may split into several distinct peaks, as summarized in[30].

It is known that incorporating Au nanoparticles into the TiO$_2$ can reduce the bandgap energy of the TiO$_2$[12]. The reduction is known due to the free electron properties exhibiting a downward shift in the conduction band and an upward shift in the valence band[32, 33]. The optical bandgap of the Au@TiO$_2$ core-shell nanoparticles (Figure 5) was in the range of 2.49-2.75 eV, which was substantially lower than that of TiO$_2$ (3.20 eV)[34] and was likely attributed to defect-induced narrow band gap[35–37]. A pronounced drop in bandgap energy of sample with the largest Au core diameter can be elucidated through Raman spectroscopy results shown in Figure 2 .

Incident photon-to-current conversion efficiency measurement was performed to investigate the spectral response of plasmon-enhanced DSSC (Figure 6). The dashed lines indicate the absorption spectra of N719 dye molecules. In general, the spectra consist of an additional peak located at 420-470 nm (marked with *). This peak is likely related to modifying electronic states
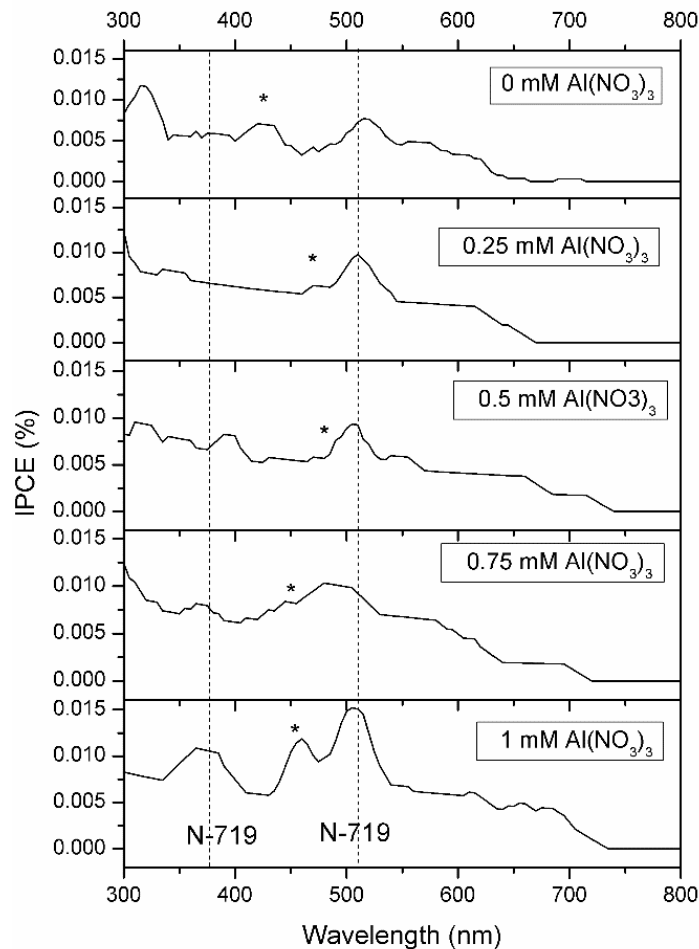
FIGURE 6 Incident photon to current conversion (IPCE) curves for core-shell Au@TiO$_2$ with the addition of Al(NO$_3$)$_3$.

Au-TiO$_2$ due to a hetero-junction-induced charge transfer interaction[30]. The presence of this peak is more obvious for the samples with core diameter >100 nm arising from the enhanced near-field effects of AuNPs.

Figure 7 shows the scattering spectra from the MNPBEM simulation. All spectra have a relatively broad resonance around 520 nm, caused by the collective plasma oscillations of the free electron gas. Figure 7 (inset) also gives a closer look at how the cross-section depends on the size of the particle. It is clear that the larger the Au diameter, the larger the cross-section obtained. Accordingly, the surface charges and real part of the induced electric field became larger, as seen in Fig 8 . It is noted that the current simulation used air as the surroundings of Au, which has refractive indices of 1. By changing the surroundings with TiO$_2$, one may obtain a redshift of the marked peak at 520 nm to 550 nm[38].

The oscillating surface charges strongly amplify the electric field of incident light in metal nanoparticles. Light absorption increases in proportion to the square of the electric field amplitude. In this research, Au nanoparticles in DSSC improved absorption of photoelectrode and generation of photocurrent, Au nanoparticles themselves are known as strong visible light absorbance.

Figure 9 illustrates the behavior of the J-V curves of the studied samples. The individual results are tabulated in Table 1 . The DSSC containing no Au@TiO$_2$ core-shell has the lowest Jsc and Voc. Hence its efficiency is also the lowest. For DSSC with Au@TiO$_2$ inclusion, the Jsc increases as the Au core diameter increases, whereas the Voc is sluggishly changed with the Au core diameter. Such an observation reveals that the mechanism responsible for the efficiency enhancement of Au@TiO$_2$ addition
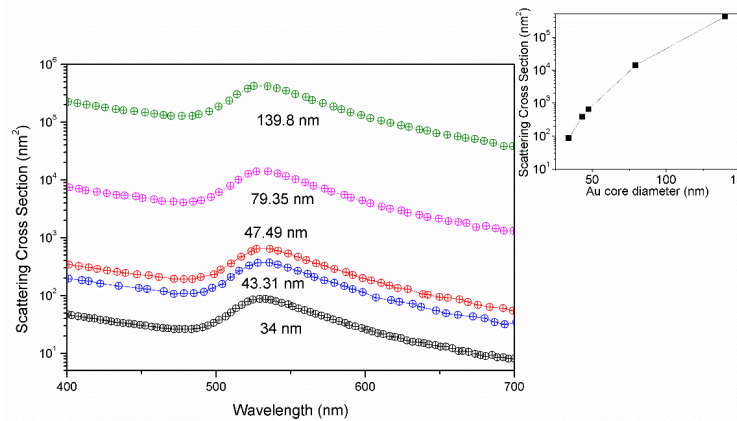
FIGURE 7 Planewave excitation of Au nanoparticles in the air for various diameters.

(a) (a)

(b) (b)
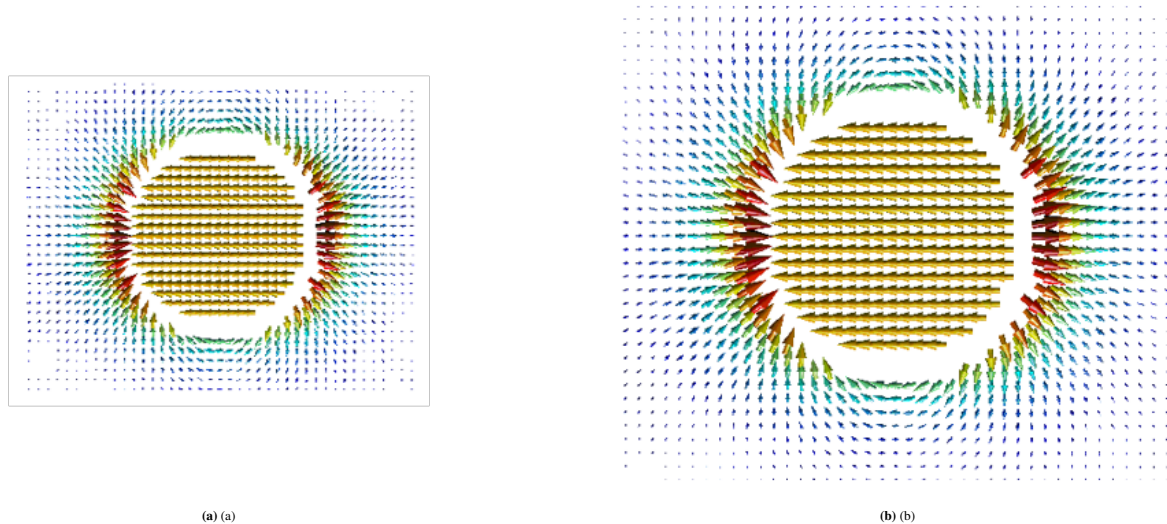
FIGURE 8 Surface charge distribution of Au produced by (a) 0.25 mM Al(NO$_3$)$_3$ 34 nm (b) 0.25 mM Al(NO$_3$)$_3$ 139 nm.

TABLE 2 The efficiency of DSSC with various diameters of Au@TiO$_2$ produced by various Al(NO$_3$)$_3$.

Types	Concentration (mM)	Jsc ($mA.cm^{-2}$)	Voc (V)	FF (%)	Efficiency (%)
Al(NO$_3$)$_3$	0.25	0.058	0.782	42.61	0.019493
	0.50	0.100	0.728	36.87	0.026006
	0.75	0.103	0.730	38.00	0.030807
	1.00	0.113	0.703	40.44	0.031312
	0.00	0.075	0.709	37.35	0.019960
TiO$_2$ pristine	-	0.038	0.700	34.28	0.008870

depends strongly on the Au core diameter. Just value itself is determined by the initial number of photogenerated charge carriers and the effectiveness in the injection of electrons from N719 dye to the conduction band of TiO$_2$.

Zhang et al. [39] The addition of Au@TiO$_2$ on TiO$_2$ induces an interfacial charge transfer process. Also, it behaves as a scattering element for plasmonic scattering to trap the light and near-field coupled with dye molecules [39], thereby increasing the Jsc value.
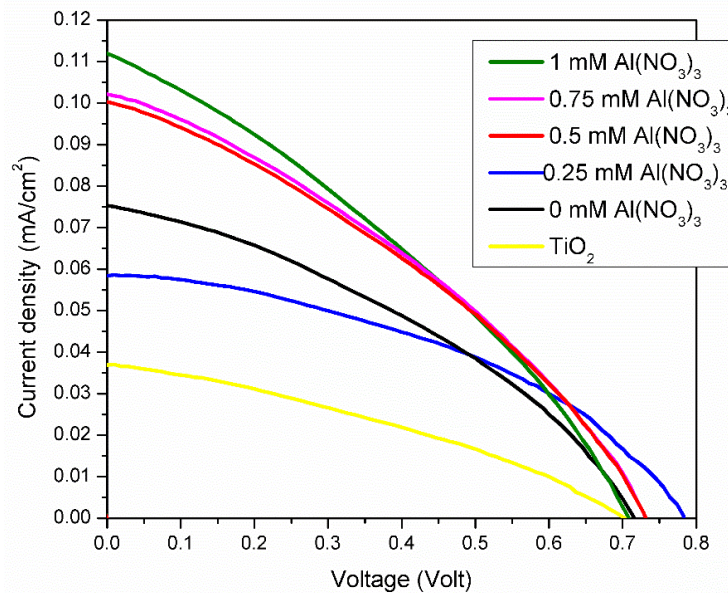
FIGURE 9 Photocurrent density – voltage curve of the DSS.

This agrees with the MNPBEM simulation, which shows that the larger the Au core size, the higher the scattering cross-section (Figure 7).

It is clear from Table 2 that Voc of Au@TiO$_2$ modified photoanodes is varied along with the change in Au core size. The increase in Voc has been attributed to the photo-charging effect due to the stored electrons in the Au core, leading to upward shifting of the TiO$_2$ Fermi level and increasing the Voc. An earlier study on the effect of Au size on TiO$_2$ photoanode showed that the smaller the metal core, the greater the Voc obtained[1, 40]. However, the change in Voc is not as significant as that of the Jsc, which could be due to the interplay between boosting the charge transfer-plasmonic scattering and modification of the Fermi level.

5 | CONCLUSION

The diameter of the Au core in Au@TiO$_2$ core-shell can be controlled by varying *Al* (NO3)3 amounts. Cell efficiency was improved with the Au@TiO$_2$ core-shell, and the increase is in line with the increase in Au core size due to the change in the scattering cross-section. The efficiency was enhanced by about twice compared to that without Au nanoparticles. The enhanced performance was largely attributed to the charge transfer process and also behaved as a scattering element for the plasmonic scattering of the Au@TiO$_2$ core-shell nanoparticles. At the same time, the change in Fermi level due to electrons' storage capability in the Au core was minor due to the presence of defects induced by $Ti - O$ bonds.

ACKNOWLEDGMENT

CREDIT

Sangsaka Wira Utama: Investigation, Data curation, Software. **Nur Fadhilah:** Conceptualization, Investigation, Data curation, Methodology, Writing-original draft preparation. **Muhammad Husain Haekal:** Data curation, Writing- Original draft

preparation, Visualization. **Rozalina Zakaria:** Supervision, Resources. **Rachmat Hidayat:** Supervision, Resources. **Doty Dewi Risanti:** Supervision, Writing-Reviewing and Editing.

References

1. Liu WL, Lin FC, Yang YC, Huang CH, Gwo S, Huang MH, et al. The influence of shell thickness of Au@TiO2 core–shell nanoparticles on the plasmonic enhancement effect in dye-sensitized solar cells. Nanoscale 2013;5(17):7953–7962. http://dx.doi.org/10.1039/C3NR02800C.

2. Wan G, Peng X, Zeng M, Yu L, Wang K, Li X, et al. The Preparation of Au@TiO2 Yolk–Shell Nanostructure and its Applications for Degradation and Detection of Methylene Blue. Nanoscale Research Letters 2017;12.

3. Qi J, Dang X, Hammond PT, Belcher AM. Highly Efficient Plasmon-Enhanced Dye-Sensitized Solar Cells through Metal@Oxide Core–Shell Nanostructure. ACS Nano 2011;5(9):7108–7116. https://doi.org/10.1021/nn201808g.

4. Crane CC, Wang F, Li J, Tao J, Zhu Y, Chen J. Synthesis of Copper-Silica Core-Shell Nanostructures with Sharp and Stable Localized Surface Plasmon Resonance. Journal of Physical Chemistry C 2017;121(10):5684–5692.

5. Toudert J, Serna R, Jiménez De Castro M. Exploring the optical potential of nano-bismuth: Tunable surface plasmon resonances in the near ultraviolet-to-near infrared range. Journal of Physical Chemistry C 2012;116(38):20530–20539.

6. Chen TM, Xu GY, Ren H, Zhang H, Tian ZQ, Li JF. Synthesis of Au@TiO2 core-shell nanoparticles with tunable structures for plasmon-enhanced photocatalysis. Nanoscale Advances 2019;1(11):4522–4528.

7. Kuddah MSM, Putra MH, Djuhana D. The thickness effect on lspr spectra of au-nanorod coated tio2 and sio2 studied by mnpbem. IOP Conference Series: Materials Science and Engineering 2019;553(1).

8. Navas J, Fernández-Lorenzo C, Aguilar T, Alcántara R, Martín-Calleja J. Improving open-circuit voltage in DSSCs using Cu-doped TiO2 as a semiconductor. physica status solidi (a) 2012 feb;209(2):378–385. https://doi.org/10.1002/pssa.201127336.

9. Dhonde M, Sahu K, Murty VVS, Nemala SS, Bhargava P. Surface plasmon resonance effect of Cu nanoparticles in a dye sensitized solar cell. Electrochimica Acta 2017;249:89–95. https://www.sciencedirect.com/science/article/pii/S0013468617316274.

10. Muduli S, Game O, Dhas V, Vijayamohanan K, Bogle KA, Valanoor N, et al. TiO2–Au plasmonic nanocomposite for enhanced dye-sensitized solar cell (DSSC) performance. Solar Energy 2012;86(5):1428–1434. https://www.sciencedirect.com/science/article/pii/S0038092X12000588.

11. Gao Y, Fang P, Chen F, Liu Y, Liu Z, Wang D, et al. Enhancement of stability of N-doped TiO2 photocatalysts with Ag loading. Applied Surface Science 2013;265:796–801. https://www.sciencedirect.com/science/article/pii/S0169433212020880.

12. Lim SP, Pandikumar A, Huang NM, Lim HN. Facile synthesis of Au@TiO2 nanocomposite and its application as a photoanode in dye-sensitized solar cells. RSC Advances 2015;5(55):44398–44407.

13. Sanad MMS, Shalan AE, Rashad MM, Mahmoud MHH. Plasmonic enhancement of low cost mesoporous Fe2O3-TiO2 loaded with palladium, platinum or silver for dye sensitized solar cells (DSSCs). Applied Surface Science 2015;359:315–322. https://www.sciencedirect.com/science/article/pii/S0169433215025258.

14. Huang LH, Sun C, Liu YL. Pt/N-codoped TiO2 nanotubes and its photocatalytic activity under visible light. Applied Surface Science 2007;253(17):7029–7035. https://www.sciencedirect.com/science/article/pii/S0169433207002334.

15. Rycenga M, Cobley CM, Zeng J, Li W, Moran CH, Zhang Q, et al. Controlling the Synthesis and Assembly of Silver Nanostructures for Plasmonic Applications. Chemical Reviews 2011 jun;111(6):3669–3712. https://doi.org/10.1021/cr100275d.

16. Sugawa K, Tahara H, Yamashita A, Otsuki J, Sagara T, Harumoto T, et al. Refractive Index Susceptibility of the Plasmonic Palladium Nanoparticle: Potential as the Third Plasmonic Sensing Material. ACS Nano 2015 feb;9(2):1895–1904. https://doi.org/10.1021/nn506800a.

17. Ng SA, Razak KA, Cheong KY, Aw KC. Memory properties of Au nanoparticles prepared by tuning HAuCl4 concentration using low-temperature hydrothermal reaction. Thin Solid Films 2016;615:84–90. https://www.sciencedirect.com/science/article/pii/S0040609016301444.

18. Ng SA, Razak KA, Cheong KY, Aw KC. The effect of Al(NO3)3 concentration on the formation of AuNPs using low temperature hydrothermal reaction for memory application. Sains Malaysiana 2016;45(8):1213–1219.

19. Mark PR. Forces and Interactions Between Nanoparticles for Controlled Structures. PhD thesis, The State University of New Jersey; 2013.

20. Zeng S, Yu X, Law WC, Zhang Y, Hu R, Dinh XQ, et al. Size dependence of Au NP-enhanced surface plasmon resonance based on differential phase measurement. Sensors and Actuators B: Chemical 2013;176:1128–1133. https://www.sciencedirect.com/science/article/pii/S0925400512009860.

21. Yoo SM, Rawal SB, Lee JE, Kim J, Ryu HY, Park DW, et al. Size-dependence of plasmonic Au nanoparticles in photocatalytic behavior of Au/TiO2 and Au@SiO2/TiO2. Applied Catalysis A: General 2015;499:47–54. https://www.sciencedirect.com/science/article/pii/S0926860X15002355.

22. Wang Y, Yang C, Chen A, Pu W, Gong J. Influence of yolk-shell Au@TiO2 structure induced photocatalytic activity towards gaseous pollutant degradation under visible light. Applied Catalysis B: Environmental 2019;251:57–65. https://www.sciencedirect.com/science/article/pii/S0926337319302784.

23. Raznjevic K. Handbook of Thermodynamic Tables and Charts. 2nd ed. Washington: Hemisphere Publishing Corporation; 1976.

24. Wagman DD, Evans W, Parker VB, Halow I, Bailey SM. Selected Values of Chemical Thermodynamic Properties. Tables for the First Thirty-Four Elements in the Standard Order of Arrangement; 1968.

25. Hohenester U, Trügler A. MNPBEM - A Matlab toolbox for the simulation of plasmonic nanoparticles. Computer Physics Communications 2012;183(2):370–381.

26. Li Y, Wang H, Feng Q, Zhou G, Wang ZS. Gold nanoparticles inlaid TiO2 photoanodes: A superior candidate for high-efficiency dye-sensitized solar cells. Energy and Environmental Science 2013;6(7):2156–2165.

27. Su C, Liu L, Zhang M, Zhang Y, Shao C. Fabrication of Ag/TiO2 nanoheterostructures with visible light photocatalytic function via a solvothermal approach. CrystEngComm 2012;14(11):3989–3999. http://dx.doi.org/10.1039/C2CE25161B.

28. Song L, Lu Z, Zhang Y, Su Q, Li L. Hydrogen-etched TiO2-x as efficient support of gold catalysts for water–gas shift reaction. Catalysts 2018;8(1).

29. Mantri K, Selvakannan PR, Tardio J, Bhargava SK. Synthesis of very high surface area Au-SBA-15 materials by confinement of gold nanoparticles formation within silica pore walls. Colloids and Surfaces A: Physicochemical and Engineering Aspects 2013;429:149–158.

30. Wu XF, Song HY, Yoon JM, Yu YT, Chen YF. Synthesis of core-shell Au@TiO2nanopartides with truncated wedge-shaped morphology and their photocatalytic properties. Langmuir 2009;25(11):6438–6447.

31. Yao GY, Liu QL, Zhao ZY. Studied Localized Surface Plasmon Resonance Effects of Au Nanoparticles on TiO2 by FDTD Simulations. Catalysts 2018;8(6):236.

32. Lim SP, Pandikumar A, Huang NM, Lim HN. Enhanced photovoltaic performance of silver@titania plasmonic photoanode in dye-sensitized solar cells. RSC Advances 2014;4(72):38111–38118.

33. Lim SP, Pandikumar A, Huang NM, Lim HN, Gu G, Ma TL. Promotional effect of silver nanoparticles on the performance of N-doped TiO2 photoanode-based dye-sensitized solar cells. RSC Advances 2014;4(89):48236–48244.

34. Dette C, Pérez-Osorio MA, Kley CS, Punke P, Patrick CE, Jacobson P, et al. TiO2anatase with a bandgap in the visible region. Nano Letters 2014;14(11):6533–6538.

35. Kalathil S, Khan MM, Ansari SA, Lee J, Cho MH. Band gap narrowing of titanium dioxide (TiO2) nanocrystals by electrochemically active biofilms and their visible light activity. Nanoscale 2013;5(14):6323–6326.

36. Khan MM, Ansari SA, Pradhan D, Ansari MO, Han DH, Lee J, et al. Band gap engineered TiO2nanoparticles for visible light induced photoelectrochemical and photocatalytic studies. Journal of Materials Chemistry A 2014;2(3):637–644.

37. Guo HL, Zhu Q, Wu XL, Jiang YF, Xie X, Xu AW. Oxygen deficient ZnO1-x nanosheets with high visible light photocatalytic activity. Nanoscale 2015;7(16):7216–7223.

38. Wijanarko A. Pemodelan localized surface plasmon resonance (LSPR) pada nanopartikel perak (Ag) dan emas (Au) menggunakan metode elemen-hingga. PhD thesis, Universitas Indonesia; 2014.

39. Zhang Q, Chou TP, Russo B, Jenekhe SA, Cao G. Aggregation of ZnO nanocrystallites for high conversion efficiency in dye-sensitized solar cells. Angewandte Chemie - International Edition 2008;47(13):2402–2406.

40. Wang Q, Butburee T, Wu X, Chen H, Liu G, Wang L. Enhanced Performance of Dye-Sensitized Solar Cells by Doping Au Nanoparticles into Photoanodes: A Size Effect Study. Journal of Materials Chemistry A 2013;1(207890):2–9.